Feasibility of electrostatic microparticle propulsion

New Journal of Physics
The open-access journal for physics

Feasibility of electrostatic microparticle propulsion

Th Trottenberg[1,3], **H Kersten**[1] **and H Neumann**[2]

[1] Institut für Experimentelle und Angewandte Physik, Christian-Albrechts-Universität, D-24118 Kiel, Germany
[2] Leibniz-Institut für Oberflächenmodifizierung, D-04318 Leipzig, Germany
E-mail: trottenberg@physik.uni-kiel.de

New Journal of Physics **10** (2008) 063012 (15pp)
Received 17 March 2008
Published 10 June 2008
Online at http://www.njp.org/
doi:10.1088/1367-2630/10/6/063012

Abstract. This paper discusses the feasibility of electrostatic space propulsion which uses microparticles as propellant. It is shown that particle charging in a plasma is not sufficient for electrostatic acceleration. Moreover, it appears technically difficult to extract charged particles out of a plasma for subsequent acceleration without them being discharged. Two novel thruster concepts are proposed. In the first one, particles with low secondary electron emission are charged using energetic electrons in the order of magnitude of 100 eV. The second concept charges the particles by contact with needle electrodes at high electrostatic potential (∼20 kV). Both methods allow the maximum possible charges on microparticles.

[3] Author to whom any correspondence should be addressed.

Contents

1. Introduction

Electrostatic propulsion has, in comparison with chemical and electrothermal propulsion, the advantage that very high exhaust speeds can be attained. The exhaust velocity is an important parameter, because it determines how much propellant is needed for a desired change of the momentum of the space vehicle. The produced momentum p_i per ion mass m_i is identical to the velocity $v_{i0} = p_i/m_i$ ('specific impulse').

Unfavorably, the kinetic energy of an exhaust ion scales as the square of its velocity, and therefore, due to the limited power provided by solar panels, the acceleration potential for xenon thrusters is typically chosen not much higher than $U_{acc} = 2\,\mathrm{kV}$. The momentum transferred by a singly charged ion for a given kinetic energy $W_i = eU_{acc}$ is $p_i = (2W_i m_i)^{1/2}$. If the frequency at which the ions are exhausted is $\dot{n}_i$, then the total thrust $T = p_i\dot{n}_i$ becomes

$$T = (2\,P_{acc}\,m_i\dot{n}_i)^{1/2}\,, \tag{1}$$

where $P_{acc} = W_i\dot{n}_i$ stands for the power used for the acceleration. In order to enhance the thrust at a fixed power P_{acc}, the mass flow rate $m_i\dot{n}_i$ has to be increased. The ejection rate $\dot{n}_i$, i.e. the ion current, is limited by space-charge effects (Child–Langmuir law) [1]. Even though the space-charge limited current density ($\propto U_{acc}^{3/2}$) can be increased to a certain degree by the acceleration–deceleration concept [2], higher ion currents require larger grid areas. For this reason, propellants with higher atomic mass m_i, typically xenon (in earlier times also mercury and cesium), are preferred in order to increase the mass flow rate. The enhanced momentum per atom and the higher total thrust, however, are bought with the less-efficient use of the propellant mass, i.e. a lower exhaust speed $v_{i0} = (2W_i/m_i)^{1/2} = 2P_{acc}/T$.

The extrapolation of the use of heavy atoms leads to molecules, nano- and microparticles as propellants. Such novel concepts are still in the stage of preliminary experiments and proposals. The most developed concept is based on field emission thrusters which are operated in the ion–droplet mixed regime (colloid thrusters) [3]. Promising, though still unrealized, are nanoparticle thrusters which extract charged particles from a suspension by means of electric fields. The functional principle has already been shown in a scaled-up experiment with spherical and needle-shaped particles of sizes from more than a millimetre down to a few tens of micrometres [4]. Very recently, a thruster which uses charged ferroelectric microparticles was suggested [5]. Ferroelectric materials have extremely large dielectric constants resulting in very high polarization charge densities at the surface when an external electric field is applied. The resulting high electric field strengths, especially at surface irregularities, can cause electron emission, evaporation of atoms and even detachment of microparticles. In the experiment, a configuration of a 1.5-mm thin $BaTiO_3$ ceramic disk between a solid back contact and a ring-shaped front electrode in vacuum was used. Sharp voltage pulses in the kilovolt (kV) range produced a metal plasma at the surface inside the ring, and video imaging revealed that a huge number of microparticles was also generated. A significant part of the thrust was attributed to the microparticle emission. Another recently published idea for microparticle propulsion is to use 'electrostatic pressure' in a dusty plasma with high dust particle density. The electrostatic pressure was defined by Avinash as the partial pressure of a dust cloud embedded in plasma and is not of thermal origin but is caused by the repulsion between the (partially shielded) dust particles [6]. It was proposed to build a propulsion chamber similar to the combustion chamber in chemical thrusters, where dust is injected into a hot (6×10^5 K) plasma. The dust would be charged in the plasma, expand due to the electrostatic pressure, and be exhausted through the nozzle [7]. However, it has not been stated so far which plasma source, plasma confinement and chamber material could be suitable.

In this contribution, we propose novel thruster concepts, which differ from the above mentioned ones. The paper is organized as follows. Firstly, techniques for charging of microparticles are described and evaluated. Secondly, options for electrostatic acceleration with respect to the charging techniques are considered. Thirdly, available particle types are discussed. Finally, two techniques are favored that are based on experiments which were performed by others without having space propulsion in mind.

2. Charging of microparticles

In this section, different charging techniques for fine particles are described and compared with regard to the achievable charge-to-mass ratio (specific charge), q_p/m_p. Besides the accelerating potential U_{acc}, the specific charge is the decisive parameter for the exhaust velocity v_{p0} of the particles.

2.1. Charging in plasma

Fine particles immersed in a plasma are typically negatively charged due to the higher electron velocities compared to the ion velocities [8, 9]. Such a system is called a complex (or dusty) plasma. The negative charge repels most of the electrons with the exception of a small fraction in the velocity distribution that has sufficient kinetic energy to overcome the potential barrier of the particle. At the charge equilibrium, the ion current balances the current of these fast

electrons ($I_i + I_e = 0$); this equilibrium potential is known from plasma probe theories as the floating potential. The charge on a particle with radius r_p can be estimated with the commonly used orbital motion limited (OML) theory for spherical probes in a collisionless plasma [10]. The ion and electron currents are functions of the particle surface potential ϕ relative to the local plasma potential and depend on the temperatures T_i and T_e, and densities n_i and n_e of ions (mass m_i) and electrons (mass m_e), respectively,

$$I_i(\phi) = +\pi r_p^2\, e n_i \left(\frac{8kT_i}{\pi m_i}\right)^{1/2} \left(1 - \frac{e\phi}{kT_i}\right), \tag{2}$$

$$I_e(\phi) = -\pi r_p^2\, e n_e \left(\frac{8kT_e}{\pi m_e}\right)^{1/2} \exp\left(\frac{e\phi}{kT_e}\right). \tag{3}$$

From the equilibrium potential $\phi = \phi_p$, the charge can be calculated as

$$q_p = 4\pi\epsilon_0\, r_p\, \phi_p, \tag{4}$$

assuming that the particle has the capacity of a sphere in vacuum. A rule of the thumb for laboratory argon plasmas with electron temperatures $kT_e = 2$–$4\,\mathrm{eV}$ is that the particle carries per micrometre of its diameter between 2000 and 4000 electrons on its surface. The surface potentials are independent of the particle size and in the range -5 to $-10\,\mathrm{V}$ relative to the plasma potential.

The attainable charge-to-mass ratios are in the order of $q_p/m_p \approx -0.5\,\mathrm{C\,kg^{-1}}$ for a $1\,\mu\mathrm{m}$ melamine formaldehyde (MF) plastic particle ($\rho = 1500\,\mathrm{kg\,m^{-3}}$). A ten times smaller particle ($2r_p = 100\,\mathrm{nm}$) of the same material reaches a hundred times higher ratio $q_p/m_p \approx -50\,\mathrm{C\,kg^{-1}}$ due to the scaling laws $q_p \propto r_p$ and $m_p \propto r_p^3$. The surface potential of the particle (and consequently q_p and q_p/m_p) strongly depends on the electron temperature T_e and is approximately proportional to the latter, i.e. $\phi_p \propto T_e$, where the coefficient depends on the ion mass and the ion temperature.

2.2. Charging with energetic electrons

The relation $q_p \propto T_e$ suggests the increasing of the electron temperature in order to obtain higher particle charges. However, no low-temperature plasma shows electron temperatures of more than a few electron volts (eV). More promising is the use of energetic electrons. In case of monoenergetic electrons with current density j_e and electron energy W_e, equation (3) simplifies to

$$\begin{aligned} I_e(\phi) &= \pi r_p^2 \left(1 + \frac{e\phi}{W_e}\right) j_e, \qquad & W_e &\geqslant -e\phi, \\ I_e(\phi) &= 0, & W_e &< -e\phi. \end{aligned} \tag{5}$$

In the first equation, the bracketed expression means the reduction of the geometrical cross section πr_p^2 due to the deflection of the electrons (OML theory). If the electrons have a sufficiently high current density j_e, then the equilibrium particle surface potential ϕ_p closely follows the potential which corresponds to the electron energy

$$\phi_p \approx -W_e/e. \tag{6}$$

Such an experiment was performed by Walch *et al* [11]. The plasma was generated with a hot filament discharge in a double plasma machine, where the filaments could be biased negatively

Table 1. Secondary electron emission data for some elements [13] and glass [11].

Material	W_1	δ_{max}
Al	300 V	1.0
C (graphite)	300 V	1.0
C (soot)	None	0.45
Cu	200 V	1.3
Fe	120 V	1.3
Si	125 V	1.1
Glass	40 V	2–3

up to −120 V to inject 2 mA of fast electrons into the chamber. The particles were dropped from the top through the chamber and collected at the bottom with a Faraday cup, which allowed the measurement of the particle charge. The gas pressure (argon at 2.7×10^{-4} Pa) was sufficiently low so that the fast electrons did not lose their energy by collisions with neutrals. Up to a critical electron energy, which was characteristic for each particle material, the particle surface potential followed the filament potential as expected, and above that critical energy, the particle charge decreased. The maximum surface potentials reported are approximately −90 V for graphite, −60 V for copper, −50 V for silicon and −40 V for glass particles.

This observation was explained by two effects. One is the collection of ions created by the higher energetic electrons by ionization collisions with the background gas, and the other is the secondary electron emission from the particle surface. While the undesired ion current can be minimized by using a lower gas density [12], the secondary electron current I_s depends on the (kinetic) primary electron energy at the particle surface $W_{ep} = W_e + e\phi$ and the secondary electron yield $\delta(W_{ep})$:

$$I_s(\phi) = -\delta(W_{ep}) I_e(\phi). \tag{7}$$

The complete equation for the charge equilibrium then reads

$$I_i(\phi) + I_e(\phi) + I_s(\phi) = 0. \tag{8}$$

The secondary electron yield has typically a maximum $\delta(W_{max}) = \delta_{max}$ at a material-specific energy W_{max}. Some materials reach $\delta(W_1) = 1 < \delta_{max}$ for an energy $W_1 < W_{max}$ (see table 1) [13]. Even though graphite particles attained the highest surface potentials in the experiment performed by Walch *et al*, this material might not be the best choice when sizes of a micrometre or less are required. Walch *et al* used much bigger particles, because the signal-to-noise ratios in the charge measurements with a Faraday cup were good only for particles larger than 35 μm. Graphite microparticles are composed of platelets and are typically not spherical due to the crystal structure [14, 15]. The corresponding sharp edges are disadvantageous, as will be shown in section 2.5.

Exemplarily, we therefore consider 1 μm and 100 nm aluminium particles charged with 90 eV electrons. Aluminium has very similar secondary electron emission properties in comparison with graphite (see table 1). The charge would be approximately 31 000 and 3100 negative elementary charges, corresponding to $q_p/m_p \approx -3.5$ and $-350\,\mathrm{C\,kg^{-1}}$, respectively ($\rho = 2700\,\mathrm{kg\,m^{-3}}$). This is only a cautious extrapolation, as the charges in the experiment of

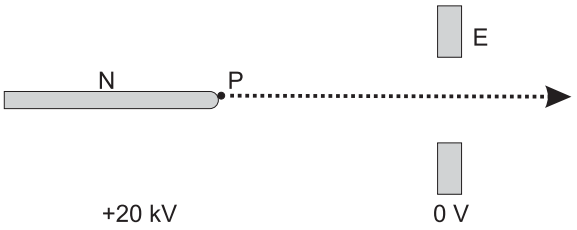

Figure 1. Simplified schematic drawing of the particle charging and accelerating device. The needle (N) charges a particle (P) which is later accelerated toward the electrode (E). The particle leaves the system through the hole in the electrode.

Walch *et al* were probably limited due to the finite ion density [11, 12]. Furthermore, metal[4] or carbon-coated spherical polymer particles can be used instead of all-metal particles in order to obtain lighter particles and higher specific charges. Carbon coatings of a few nanometres (nm) are commonly used in the sample preparation techniques for electron microscopy.

2.3. Charging by contact with high-voltage needle electrodes

Hypervelocity experiments for the simulation of micrometeorites and their impacts for example on the surface of the moon, space vehicles, spacesuits and instruments also use electrostatic acceleration of charged microparticles. A successful technique applied there allows the highest possible specific charges (see section 2.5). The particles are charged by contact with very small spherical or needle-shaped surfaces at high-voltage potentials, as indicated in figure 1. Shelton *et al* [16] applied this technique using a tapered tungsten wire with a diameter of $2r_n = 24\,\mu$m at the tip as a charging electrode, which is maintained at a positive potential of $U_n = +20\,$kV. When a microparticle ($r_p < r_n$) touches the needle tip, it acquires the charge

$$q_p = \frac{2}{3}\pi^3 \epsilon_0 r_n \frac{r_p^2}{(r_p + r_n)^2} U_n, \tag{9}$$

with the assumption of a spherical 'needle tip'. For $r_n \gg r_p$, the electric field strength on the particle becomes $E_p = \pi^2 U_n / 6 r_n$ after separation from the electrode. For example, a needle tip with radius $r_n = 12\,\mu$m at a potential $U_n = +20\,$kV yields an electric field strength of $E_p = 2.7 \times 10^9\,\mathrm{V\,m^{-1}}$. According to equation (9), a 1 μm iron particle ($\rho = 7874\,\mathrm{kg\,m^{-3}}$) would carry 440 000 positive elementary charges and have a specific charge of $q_p/m_p = +17\,\mathrm{C\,kg^{-1}}$. The values for the smaller 100 nm particle are $q_p = +4700e$ and $q_p/m_p = +180\,\mathrm{C\,kg^{-1}}$.

Dielectric particles can also be charged with this technique, but they have to be coated with a conducting material. In the Heidelberg dust accelerator, coated latex particles were successfully used [17]. Table 2 shows some of the experimental values for iron and latex particles. The latex particles had a narrow size distribution centered about 0.75 μm, and most of the particles were accelerated to speeds between 5 and 11 $\mathrm{km\,s^{-1}}$. The size distribution of the iron powder was broad (0.2–2.4 μm) resulting in speeds from less than 1 $\mathrm{km\,s^{-1}}$ to more than 10 $\mathrm{km\,s^{-1}}$.

[4] Microparticles GmbH, Berlin, http://www.microparticles.de.

Table 2. Experimental parameters for contact charging in a dust source with a needle electrode. Mass m_p and speed v_{p0} were selected from speed–mass distributions of about 20 000 iron and 2840 latex particles published in [17], the other parameters were calculated. The particles were accelerated with a potential of $U_{acc} = 2$ MV.

Material	m_p (kg)	v_{p0} (km s^{-1})	$2r_p$ (μm)	q_p/m_p (C kg^{-1})	q_p (e)	E_p (V m^{-1})
Iron	10×10^{-16}	4	0.62	+4.0	+25 000	0.4×10^9
Iron	10×10^{-16}	10	0.62	+25	+160 000	2.3×10^9
Latex	2.4×10^{-16}	5	0.75	+6.3	+9400	0.1×10^9
Latex	2.4×10^{-16}	11	0.75	+30	+45 000	0.5×10^9

2.4. Charging in quadrupole traps

Quadrupole traps together with electron and ion beams have been used to charge microparticles for subsequent acceleration [18], and for the study of charging processes [19]–[22], particle fragmentation [23], and dust sputtering [22]. The trap allows to keep the particle in the beam and to determine very accurately its specific charge by a measurement of the grain oscillation frequency. Vedder [18] was able to reach positive charge-to-mass ratios of up to 400 C kg^{-1} by applying a beam of positive ions. Negative charging is limited due to secondary electron emission. Electron beams with energies where the secondary electron emission yield is higher than unity produced positive surface potentials in the range of a few volts, which has also been confirmed by Pavlu *et al* [22].

However, particle trapping in quadrupoles is technically quite costly. Only a single particle or perhaps a few can be charged and confined at the same time. Vedder stated referring to his experiment that 'probably four good shots a day could be expected' [18]. For this reason, charging in quadrupole traps is not further considered in this paper as a technique which could be useful for electric propulsion.

2.5. Upper limits for the particle charge

The electric charge on a microparticle is limited by two processes which become important at very high electric field strength on the particle surface [24]. For negative charges, the electron field emission begins at $|E_p| > 10^9$ V m^{-1}. For positive charges field evaporation destroys the particle, if $|E_p| > 10^{10}$ V m^{-1}. In the case of materials with low tensile strength or even fluffy grains, charges of both signs are able to fragment the particles ('Coulomb explosion') [23] even at lower field strengths.

The specific charge q_p/m_p, which is the crucial parameter for electrostatic acceleration, can be related to the electric field at the surface $E_p = q_p / 4\pi\epsilon_0 r_p^2$, assuming spherical particles. By means of the particle mass $m_p = \frac{4}{3}\pi r_p^3 \rho$, one obtains the specific charge as

$$\frac{q_p}{m_p} = 3\frac{\epsilon_0 E_p}{r_p \rho}. \tag{10}$$

This equation can be used to calculate the maximum possible specific charge, which depends on the particle size and density and the critical electric field strengths for positive and negative

Table 3. Estimated range of the possible specific charges for spherical particles with different materials and sizes. The critical electric field strengths have been assumed cautiously to be $10^9\,\mathrm{V\,m^{-1}}$ for negative and $10^{10}\,\mathrm{V\,m^{-1}}$ for positive charges [24].

Material	$\rho\,(\mathrm{kg\,m^{-3}})$	$2r_\mathrm{p} = 1.0\,\mu\mathrm{m}\,(\mathrm{C\,kg^{-1}})$	$2r_\mathrm{p} = 0.1\,\mu\mathrm{m}\,(\mathrm{C\,kg^{-1}})$
Latex	1100	$(-48 + \cdots + 480)$	$(-480 + \cdots + 4800)$
MF	1500	$(-35 + \cdots + 350)$	$(-350 + \cdots + 3500)$
Aluminium	2700	$(-20 + \cdots + 200)$	$(-200 + \cdots + 2000)$
Iron	7874	$(-6.7 + \cdots + 67)$	$(-67 + \cdots + 670)$

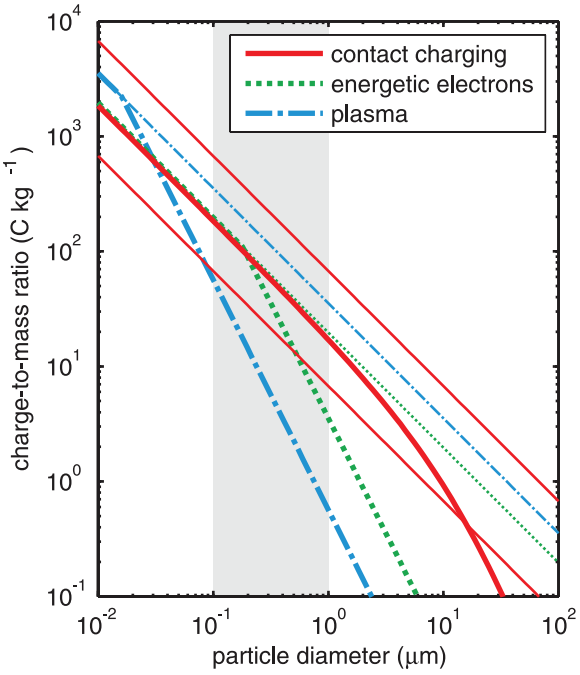

Figure 2. Comparison of three different charging techniques, i.e. contact charging of iron particles with a 24 μm needle tip at 20 kV, charging of aluminium particles with 90 eV electrons and charging of MF particles in plasma to a surface potential of -8 V. The bold lines indicate the highest possible specific charges, and the fine lines of respectively the same style show the limit for electron field emission and in the case of the contact charging method also the limit for field evaporation (upper line). The gray shaded bar highlights particle sizes from 100 nm to 1 μm.

charges. Table 3 shows the charge-to-mass ratios for some combinations of size and material assuming that the abovementioned critical field strengths are the same for all the particles and that the particles are spheres. The table reveals, for example, that the expected charge-to-mass ratio of $-350\,\mathrm{C\,kg^{-1}}$ for the 100 nm aluminium particle (section 2.2) is not realistic, because electron field emission limits the specific charge to $-200\,\mathrm{C\,kg^{-1}}$ or less.

Figure 2 compares the expected charge-to-mass ratios for three considered charging techniques. Electron field emission limits the charge of the aluminium particles charged by

energetic electrons for radii below 200 nm. In the case of iron particles charged by contact with a 20 kV needle, electron field emission would limit negative charging, meanwhile positively charged particles are not yet affected by field evaporation.

3. Acceleration of charged microparticles

In order to make the particles useful for propulsion, they have to be accelerated by an electric field. The desired exhaust velocity determines the required acceleration voltage U_{acc} by means of the equation

$$\tfrac{1}{2} m_{\mathrm{p}} v_{\mathrm{p0}}^2 = |U_{\mathrm{acc}} q_{\mathrm{p}}|. \tag{11}$$

In the following, the challenges and attainable exhaust velocities are discussed.

3.1. Particles charged in plasma

3.1.1. Plasma with low degree of ionization. Plasmas, which are generated by electron–neutral collisions, like dc glow discharges, thermionic discharges, capacitively or inductively coupled rf discharges, and electron cyclotron resonance (ECR) plasmas produced by microwaves, show ionization degrees of only a few percent or less. If the microparticles are charged in such a plasma, the acceleration cannot be accomplished in the plasma for the following reason. If an acceleration electrode is at low potential, it collects ions and electrons from its disturbed vicinity like a Langmuir probe. Due to the extremely low mobility of the particles, the electron current would be much higher than the current of the particle charges, and only a vanishing portion of the power would be deposited in the microparticle motion. A high-voltage electrode instead would lead to a secondary discharge or electrical breakdown with the same effect. This means that the plasma has to be switched off or the microparticles have to be moved out of the plasma in order to be accelerated.

After switch-off of the plasma the particle charge can possibly be conserved, but only if the gas pressure is very low and the particles are not densely packed [25]. In a microgravity experiment on the International Space Station, where these conditions were not fulfilled, the remaining charge after the switch-off was two orders of magnitude below the initial charge [25]. In an on-ground experiment performed with a chamber which was constructed in the same way ('PKE-Nefedov' chamber), 200 nm dust particles kept residual charges in the range of only $q_{\mathrm{p}} = -12e \cdots +2e$, when the discharge was abruptly switched off [26]. This was again two orders of magnitude below the initial charge. Furthermore, if there is remaining neutral gas in a particle accelerator, the electric field for acceleration would again generate a glow or an arc discharge.

Moving the particles out of the plasma for further acceleration can be performed in two different ways. The first possibility is by using a grid, which limits the plasma like in an ion-thruster. The particle would traverse the positive space charge in the plasma sheath, and would therefore at least partially be discharged [9, 27]. Some of the particles would collide with the grid, lose charge and become useless for propulsion. The second possibility is extracting the particles through a diffuse edge of the plasma, i.e. where no walls limit the plasma. The particle would see an always quasineutral plasma with decreasing density. This was the case in the already mentioned experiment [11], where the particles kept the entire expected charge.

To judge if charging in plasma is suitable for electrostatic propulsion with microparticles, we can consider a 0.5 μm particle. An acceleration potential of 2 kV yields an exhaust speed of only 95 m s^{-1}; and the modest exhaust speed $v_{p0} = 500\,\mathrm{m\,s^{-1}}$, which is in the range of cold gas thrusters, would already require an accelerating voltage of $U = 55\,\mathrm{kV}$.

3.1.2. Fully ionized plasma. A nearly fully ionized (low-temperature) plasma can be produced with cesium vapor and a hot tungsten surface similar to the technique applied in early cesium ion thrusters [2] and Q machines [28]. The advantage is that no neutral gas would impose a limit on the acceleration field strength because of electrical breakdown. It appears possible to apply an intermittent acceleration voltage to appropriately designed electrodes in the plasma, accepting the unavoidable side effect of the run-off of the plasma to the electrodes and the related currents. The disadvantages are that cesium is a highly corrosive alkali metal which limits the lifetime of the thruster, and that the electrons have only the temperature T_e ($= T_i$) of the tungsten surface, typically 2000 K or 0.2 eV. Due to equations (2) and (3) and the resulting approximate relation $\phi_p \propto T_e$, the particles carry only 270 elementary charges per micrometre of diameter.

Due to the relation $q_p \propto T_e$, the attainable particle charges are at least ten times lower than that in a plasma with electron temperatures ranging from 2 to 4 eV. According to equation (11), the exhaust speeds turn out to be at least three times lower, unless the accelerating potential chosen is one order of magnitude higher.

3.2. Particles charged by energetic electrons

The already mentioned experiment performed by Walch *et al* with energetic electrons from a biased hot filament was operated at a very low gas pressure ($<3 \times 10^{-4}$ Pa) and low plasma density so that the charging was dominated by the fast electrons [11]. The background gas and the plasma, which is generated by the fast electrons, are actually unnecessary for the charging process. The difficulties mentioned in section 3.1 related to the background gas can therefore be avoided using no gas. Acceleration can be achieved with additional ring or cylinder anodes. A transverse magnetic field can be applied to prevent the electrons from being accelerated by the electric field. A gyroradius $r_{ce} = 1\,\mathrm{mm}$ for a 90 eV electron is already obtained for a weak magnetic field of $B = 32\,\mathrm{mT}$ and is sufficiently small to guide the electrons along the magnetic field lines if the dimensions of the electrodes are much bigger than the gyroradius. The microparticles, on the other hand, are not magnetized due to their much lower specific charge q_p/m_p. They can cross the magnetic field lines and follow the accelerating electric field.

Aluminium particles charged with the energetic electron technique can be accelerated to much higher speeds than the particles charged in a plasma, as shown in figure 3. Particles of 0.5 μm size reach the exhaust speed of cold gas thrusters ($v_{p0} \approx 500\,\mathrm{m\,s^{-1}}$) at an acceleration potential of 7200 V. Five times smaller particles (100 nm) would reach exhaust velocities comparable to chemical engines ($v_{p0} \approx 3200\,\mathrm{m\,s^{-1}}$), if an acceleration potential of 60 000 V is applied.

3.3. Particles charged by contact with needle electrodes

When the particles leave the dust source, they have already been accelerated by the potential difference between the needle and hole electrode. In the case of the Heidelberg dust

Table 4. Expected exhaust speeds for particles charged by contact with a high-voltage needle electrode. The values for $U_{acc} = 20\,kV$ correspond to the source without further acceleration, the designation $U_{acc} = 200\,kV$ means the sum of 20 kV needle potential plus a 180 kV additional accelerator potential. The charge-to-mass ratios are the same as in table 2.

Material	Iron	Latex
m_p (10^{-16} kg)	10	2.4
$2r_p$ (μm)	0.62	0.75
q_p/m_p (C kg^{-1})	+25	+30
v_{p0} (km s^{-1}) at $U_{acc} = 20\,kV$	1.0	1.1
v_{p0} (km s^{-1}) at $U_{acc} = 200\,kV$	3.2	3.5

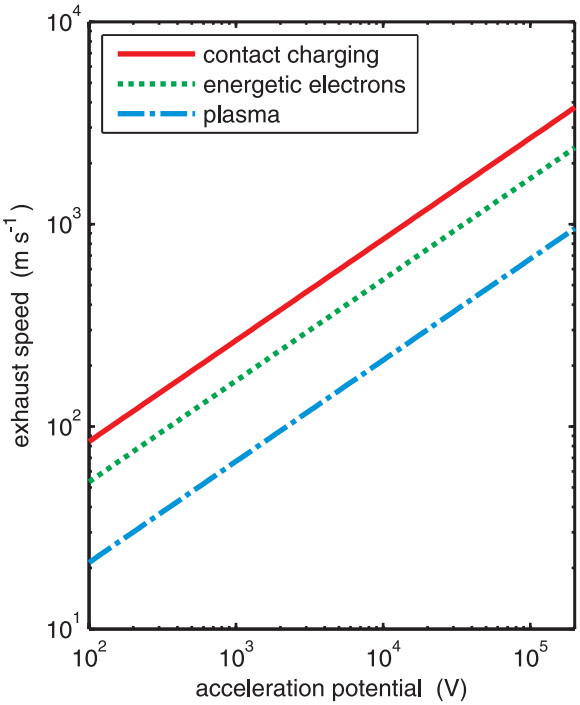

Figure 3. Calculated exhaust speeds for 0.5 μm particles (parameters as in figure 2). The specific charges are +37 C kg^{-1} (contact charging), −14 C kg^{-1} (energetic electrons) and −2.3 C kg^{-1} (plasma). The distance of the upper two lines corresponds to a factor of 1.6.

accelerator [17], a subsequent acceleration with 20 kV or 2 MV was accomplished, but this is not necessary.

In table 4, the performance of the particle source without and with an additional accelerating system is shown. The source alone surpasses cold gas thrusters in exhaust speed, and with a further 180 kV acceleration the microparticle thruster becomes comparable with chemical thrusters. Accelerating potentials in the range of 10^5 V should not be a problem technically [2].

4. Propellant material

4.1. Spherical particles

Microparticles made of melamine, silica and other materials are available with nearly perfect spherical shape, narrow size distributions and optional metal coatings (see footnote 4). Spherical particles are advantageous with respect to charging and handling for the following reasons.

The two charging techniques which use energetic electrons and needle electrodes allow particle charges close to the theoretical limits defined by electron field emission and field evaporation. These limits are highest for spherical particles, because there the charges are uniformly distributed over the surface. If the shape deviates from a sphere, the charge density and consequently the field strength decrease on some parts of the surface and increase on others. In the high-field regions, especially at sharp edges, field emission and evaporation would then occur at lower particle charges. For this reason spherical particles are to be preferred.

Moreover, monodisperse spherical particles are easier to handle. From the authors' experience, dry MF particles with at least 0.5 μm diameter do not clump and behave like a liquid in a container. Amorphous powder particles with a broad size distribution tend to clog much more. This effect is known from granular materials as 'jamming' [29]. However, the smaller the particles are, the more important the cohesive forces become as an additional effect so that spherical particles also agglomerate. For this reason manufacturers of monodisperse microparticles deliver particles smaller than 500 nm in aqueous suspensions (see footnote 4).

4.2. On-board synthesized particles

Particle formation in reactive and etching plasmas, e.g. with methane, silane and acetylene, is well known [30] so that one can think about the production of particles on board. Generation of the plasma where the particles are formed consumes additional energy which debits the efficiency of the thruster and causes additional weight for the plasma reactor and necessary electronics. But there are also some advantages over prefabricated particles, e.g. clumping of stored particles and congestion of tank and ducts as possible problems would be avoided. However, the authors think that it is untimely to discuss the concept of on-board production in detail before a thruster works with well-defined model particles.

4.3. Hollow particles

Hollow glass microspheres ('microballoons') are known as low-priced fillers in composite materials like light-weight concrete. Figure 4(a) shows the nearly perfect spherical shape of the microspheres. The particle in figure 4(b) was intentionally broken to show the very thin walls, which are approximately 300 nm thick. The lower overall mass density of a hollow microparticle can yield higher specific charges.

Firstly, we consider the maximum possible specific charge limited by the field strength $E_{\mathrm{p,max}}$ corresponding to one of the two effects discussed above. Similar to equation (10), the charge-to-mass ratio can be recalculated for a hollow sphere with radius $r_{\mathrm{p,h}}$, wall thickness $d_{\mathrm{p}} \ll r_{\mathrm{p,h}}$, material density ρ_{h} and particle mass $m_{\mathrm{p,h}} = 4\pi r_{\mathrm{p,h}}^2 d_{\mathrm{p}} \rho_{\mathrm{h}}$

$$\frac{q_{\mathrm{p,h}}}{m_{\mathrm{p,h}}} = \frac{\epsilon_0 E_{\mathrm{p,max}}}{d_{\mathrm{p}} \rho_{\mathrm{h}}}. \tag{12}$$

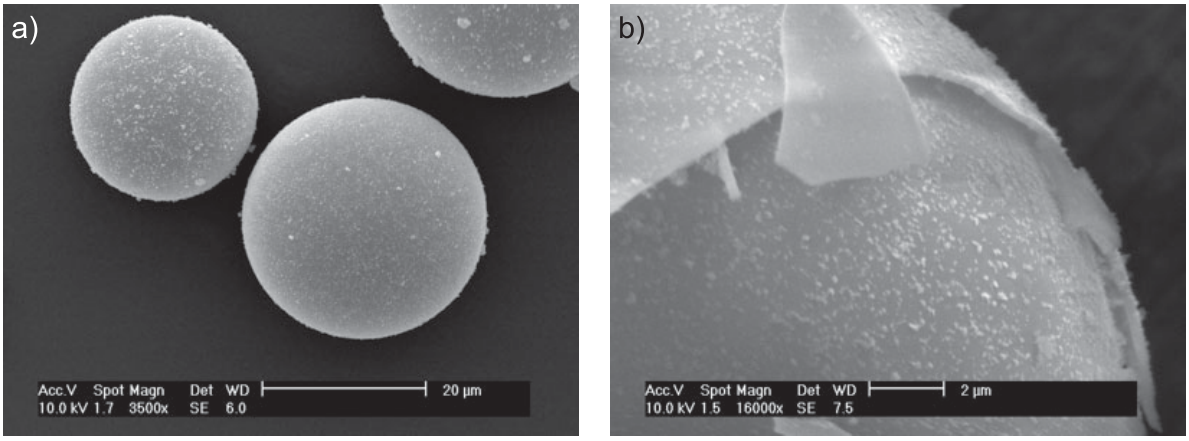

Figure 4. Hollow microspheres. The scanning electron microscope pictures show (a) the perfect spherical shape, and (b) the thin walls of a broken particle.

It is noteworthy that the charge-to-mass ratio does not depend on the particle radius $r_{\mathrm{p,h}}$, and it is now the wall thickness d_{p} which determines the specific charge. A comparison of equation (10) with equation (12) for a filled sphere with radius $r_{\mathrm{p,f}}$ and density ρ_{f} results in a higher specific charge for a hollow sphere, if $d_{\mathrm{p}} < \frac{1}{3}\frac{\rho_{\mathrm{f}}}{\rho_{\mathrm{h}}} r_{\mathrm{p,f}}$. A hollow glass microsphere with 300 nm walls and arbitrary radius has therefore only a better charge-to-mass ratio than a glass pearl bigger than 1.8 μm. But hollow microspheres made of another material and with a modified method of production might have even thinner walls and be better suited as propellant.

Secondly, we consider the specific charge of the hollow sphere for a given surface potential $\phi_{\mathrm{p,h}}$. This is the situation when the field strength limits are not reached. Using equation (4), one obtains the specific charge of the hollow sphere

$$\frac{q_{\mathrm{p,h}}}{m_{\mathrm{p,h}}} = \frac{\epsilon_0 \phi_{\mathrm{p,h}}}{d_{\mathrm{p}} r_{\mathrm{p,h}} \rho_{\mathrm{h}}}. \tag{13}$$

For comparison, the filled sphere has the charge-to-mass ratio

$$\frac{q_{\mathrm{p,f}}}{m_{\mathrm{p,f}}} = 3\frac{\epsilon_0 \phi_{\mathrm{p,f}}}{r_{\mathrm{p,f}}^2 \rho_{\mathrm{f}}}. \tag{14}$$

The hollow sphere has a higher specific charge, if $d_{\mathrm{p}} r_{\mathrm{p,h}} < \frac{1}{3}\frac{\rho_{\mathrm{f}}}{\rho_{\mathrm{h}}} r_{\mathrm{p,f}}^2$. The hollow microspheres with 300 nm walls have therefore no significant advantage over a massive particle with $2r_{\mathrm{p,f}} \approx 1\ \mu$m in this case.

4.4. Interplanetary dust particles

Finally, one might think about taking advantage of the dust which naturally exists in interplanetary space [31]. The higher dust densities in planetary rings and in the tails of comets could be sufficient to be collected by a space vehicle, which then uses the dust particles for electrostatic propulsion. Even though these particles do not fulfill the requirements on shape and stability for optimal charging, a less-efficient use of the abundant material could be accepted. However, such advanced concepts are far beyond the scope of this feasibility study.

5. Conclusion

In this paper, we made an attempt at a better understanding of the basic technical and physical aspects with respect to the feasibility of electrostatic microparticle thrusters. Spherical particles with sizes between 100 nm and 1 μm seem to be suitable for electrostatic propulsion. Bigger particles yield too low specific charges, and smaller particles agglomerate.

The estimates (see figure 3) show that particle charging in a plasma is not practicable for two reasons. Firstly, the attainable charge-to-mass ratios are too low for the considered particle sizes. Manageable acceleration potentials, perhaps up to the range of 100 kV [2], would barely yield exhaust speeds comparable to cold gas thrusters, which then are to be preferred because of their compactness and simpleness. Secondly, there are no ready-to-use techniques for extracting the particles out of the plasma which preserve the particle charge.

Two different charging mechanisms have been considered, which give ideas for two novel microparticle thruster concepts. The first one charges the particles negatively with energetic electrons. The electron energy is adjusted with regard to the secondary electron emission of the particle material so that the impacting electrons do not produce too many secondaries which would discharge the particle. This technique yields about ten times higher charges than that in plasma, if materials like aluminium or amorphous carbon with low secondary electron emissions are chosen. Since this method yields specific charges inversely proportional to the square of the particle diameter, this technique is more suited for submicron particles. The second concept uses high-voltage needle electrodes to charge the conducting particles positively or negatively, and is known from accelerators for the simulation of micrometeorites. Here, charging and acceleration are both done in one small electrode assembly. This concept allows the highest specific charges, which are only limited by field evaporation, electron field emission and Coulomb explosion in the case of fluffy grains. While the existing dust accelerators are not optimized for high ejection rates, a thruster would probably use a miniaturized needle array instead of a single needle electrode. The authors plan to perform preliminary experiments for both concepts in the near future.

Acknowledgment

This work was supported by the German Aerospace Center DLR (project no 50 JR 0644).

References

[1] Child C D 1911 Discharge from hot CaO *Phys. Rev.* I **32** 492
[2] Jahn R G 1968 *Physics of Electric Propulsion* (New York: McGraw-Hill)
[3] Lozano P and Martínez-Sánchez M 2003 Studies on the ion-droplet mixed regime in colloid thrusters *PhD Thesis* Department of Aeronautics and Astronautics, MIT
[4] Musinski L, Liu T, Gilchrist B, Gallimore A and Keidar M 2007 Nanoparticle field extraction thruster (nanoFET): design and results of the microparticle emitter prototype *Proc. Int. Electr. Propulsion Conf.* IEPC-2007-80
[5] Yarmolich D, Vekselman V and Krasik Y E 2008 A concept of ferroelectric microparticle propulsion thruster *Appl. Phys. Lett.* **92** 081504
[6] Avinash K 2006 Equation of state for the 'electrostatic pressure' in dusty plasmas *Phys. Plasmas* **13** 012109
[7] Avinash K and Zank G P 2007 Micropropulsion in space via dust-plasma thruster *Phys. Plasmas* **14** 053507

[8] Fortov V E, Ivlev A V, Khrapak S A, Khrapak A G and Morfill G E 2005 Complex (dusty) plasmas: current status, open issues, perspectives *Phys. Rep.* **421** 1
[9] Trottenberg T, Melzer A and Piel A 1995 Measurement of the electric charge on particulates forming Coulomb crystals in the sheath of a radiofrequency plasma *Plasma Sources Sci. Technol.* **4** 450
[10] Mott-Smith H M and Langmuir I 1926 The theory of collectors in gaseous discharges *Phys. Rev.* **28** 727
[11] Walch B, Horányi M and Robertson S 1995 Charging of dust grains in plasma with energetic electrons *Phys. Rev. Lett.* **75** 838
[12] Nam C-H, Hershkowitz N, Cho M H, Intrator T and Diebold D 1988 Multiple valued floating potentials of Langmuir probes *J. Appl. Phys.* **63** 5674
[13] Lide D R (ed) 2006 *CRC Handbook of Chemistry and Physics* (Boca Raton, FL: CRC Press) chapter 12 p 115
[14] LI J L, Wang L J and Jiang W 2006 Carbon microspheres produced by high energy ball milling of graphite powder *Appl. Phys.* A **83** 385
[15] Zhu H, Zhang C, Tang Y, Wang J, Ren B and Yin Y 2007 Preparation and thermal conductivity of suspensions of graphite nanoparticles *Carbon* **45** 226
[16] Shelton H, Hendricks C D Jr and Wuerker R F 1960 Electrostatic acceleration of microparticles to hypervelocities *J. Appl. Phys.* **31** 1243
[17] Stübig M, Schäfer G, Ho T-M, Srama R and Grün E 2001 Laboratory simulation improvements for hypervelocity micrometeorite impacts with a new dust particle source *Planet. Space Sci.* **49** 853
[18] Vedder J F 1963 Charging and acceleration of microparticles *Rev. Sci. Instrum.* **34** 1175
[19] Pinter S, Svestka J and Grün E 1990 Investigation of the electrostatic charging of dust particles in a Paul-trap *Astrophys. Space Sci.* **171** 217
[20] Cermak I, Grün E and Svestka J 1995 New results in studies of electric charging of dust particles *Adv. Space Res.* **15** 59
[21] Spann J F, Abbas M N, Venturini C C and Comfort R H 2001 Electrodynamic balance for studies of cosmic dust particles *Phys. Scr.* T **89** 147
[22] Pavlu J, Richterova I, Nemecek Z, Safrankova J and Cermak I 2008 Interaction between single dust grains and ions or electrons: laboratory measurements and their consequences for the dust dynamics *Faraday Discuss.* **137** 139
[23] Svestka J, Cermak I and Grün E 1993 Electric charging and electrostatic fragmentation of dust particles in laboratory *Adv. Space Res.* **13** 199
[24] Müller E W 1956 Field desorption *Phys. Rev.* **102** 618
[25] Ivlev A V *et al* 2003 Decharging of complex plasmas: first kinetic observations *Phys. Rev. Lett.* **90** 055003
[26] Couëdel L, Mikikian M, Boufendi L and Samarian A A 2006 Residual dust charges in discharge afterglow *Phys. Rev.* E **74** 026403
[27] Samarian A A, James B W, Vladimirov S V and Cramer N F 2001 Self-excited vertical oscillations in an rf-discharge dusty plasma *Phys. Rev.* E **64** 025402
[28] Rynn N and D'Angelo N 1960 Device for generating a low temperature, highly ionized cesium plasma *Rev. Sci. Instr.* **31** 1326
[29] Duran J 2000 *Sands, Powders, and Grains: An Introduction to the Physics of Granular Materials* (Berlin: Springer)
[30] Hollenstein C 2000 The physics and chemistry of dusty plasmas *Plasma Phys. Control. Fusion* **42** R93
[31] Grün E, Gustafson B A S, Dermott S and Fechtig H (ed) 2001 *Interplanetary Dust* (Berlin: Springer)